

Fig. 4. Three-dimensional model of slip on the subduction interface. Dashed lines are depth contours of the interface. Slip direction is set constant at 235°, the direction of motion of the North America plate with respect to the Juan de Fuca plate. Dark shading indicates the plate interface area with full (2.1 cm) slip; lighter shading indicates area where slip tapers linearly from 2.1 cm to 0 cm up-dip. Panels, marked by the day of year 1999, show the total area of slip on the interface in three time slices and the commensurate evolution of the surface displacement vectors [broad (yellow) = model; thin (red) with error ellipses = observed]. Day 240 is within the time interval of the GPS transient at PGC5 and ALBH, and their observed displacement vectors have been scaled, assuming a linear increase of the displacement with time.

nism for a great subduction thrust earthquake. The process of deep slip leading to a thrust earthquake is considered responsible for the 1960 ($M_w = 9.5$) Chilean earthquake (12) and the 1944 and 1946 (both $M_w = 8.2$) Nankai Trough earthquakes (13), and suggests that enhanced seismic hazard may accompany silent slip events. Denser continuous GPS networks spanning Puget Sound and Georgia Strait could characterize the timing and spatial distribution of episodic silent slip, thereby allowing real-time monitoring of the seismic potential of the subduction megathrust.

References and Notes

1. B. F. Atwater *et al.*, *Earthquake Spectra* **11**, 1 (1996).
2. K. Satake, K. Shimazaki, Y. Tsuji, K. Ueda, *Nature* **378**, 246 (1996).
3. H. Dragert, R. D. Hyndman, *Geophys. Res. Lett.* **22**, 755 (1995).
4. G. Khazaradze, A. Qamar, H. Dragert, *Geophys. Res. Lett.* **26**, 3153 (1999).
5. M. M. Miller *et al.*, *Tectonics* **20**, 161 (2001).
6. H. Dragert, R. D. Hyndman, G. C. Rogers, K. Wang, *J. Geophys. Res.* **99**, 653 (1994).
7. J. A. Henton, thesis, University of Victoria, British Columbia, Canada (2000).
8. R. M. McCaffrey, M. D. Long, C. Goldfinger, P. C. Zwick, *Geophys. Res. Lett.* **27**, 3117 (2000).
9. M. H. Murray, M. Lisowski, *Geophys. Res. Lett.* **27**, 3631 (2000).
10. R. D. Hyndman, K. Wang, *J. Geophys. Res.* **98**, 2039 (1993).
11. W. Thatcher, *Nature* **299**, 12 (1982).
12. A. T. Linde, P. G. Silver, *Geophys. Res. Lett.* **16**, 1305 (1989).
13. A. T. Linde, I. S. Sacks, M. T. Gladwin, M. J. S. Johnston, P. G. Silver, *Eos* **79**, F600 (1998).
14. G. Ranalli, H. H. Schloessin, *Geophys. Monogr. Am. Geophys. Union* **49**, 55 (1989).
15. Twelve of the 14 sites analyzed use stable, geodetic-quality monuments, either concrete piers anchored directly into bedrock, or deeply anchored drilled-and-braced monuments (29). Antennas at SEAT and LIND are mounted on roofs of large buildings, but their data show noise characteristics similar to the other sites. All sites have well-documented histories of site activity, allowing the recognition of potential disruption of their time series due to instrumental changes.
16. The Bernese GPS Software Version 4.2 (30) is used for data analysis with the following strategy: DRAO is used as a fixed reference site; precise IGS (International GPS Service) satellite orbits are used and kept fixed; ionospheric-free phase solutions are used to determine relative positions of network sites; phase ambiguities are resolved and fixed to integer values; tropospheric zenith delay is estimated hourly with no a priori tropospheric model and using a dry Niell tropospheric mapping function; tropospheric gradi-

- ents (tilt direction of the mapping function) are estimated every 6 hours; a nominal 10° cut-off elevation is used for satellites; and solid Earth tide, pole tide, and ocean loading corrections are applied.
17. R. E. Wells, C. S. Weaver, R. J. Blakely, *Geology* **26**, 759 (1998).
18. K. Wang, *Geophys. Res. Lett.* **23**, 2021 (1996).
19. T. S. James, J. J. Clague, K. Wang, I. Hutchinson, *Quat. Sci. Rev.* **19**, 1527 (2000).
20. P. Flück, R. D. Hyndman, K. Wang, *J. Geophys. Res.* **102**, 20539 (1997).
21. Y. Okada, *Bull. Seismol. Soc. Am.* **75**, 1135 (1985).
22. K. Wang, T. Mulder, G. C. Rogers, R. D. Hyndman, *J. Geophys. Res.* **100**, 12907 (1995).
23. S. Ozawa, M. Murakami, T. Tada, *J. Geophys. Res.* **106**, 787 (2001).
24. K. Heki, S. Miyazaki, H. Tsuji, *Nature* **386**, 595 (1997).
25. T. Sagiya, *Eos* **78**, F165 (1997).
26. A. T. Linde, M. T. Gladwin, M. J. S. Johnston, R. L. Gwyther, R. G. Bilham, *Nature* **383**, 65 (1996).
27. H. Hirose, K. Hirahara, F. Kimata, N. Fujii, S. Miyazaki, *Geophys. Res. Lett.* **26**, 3237 (1999).
28. K. Wang, R. D. Hyndman, M. Yamano, *Tectonophysics* **248**, 53 (1995).
29. J. O. Langbein, A. F. Wyatt, A. H. Johnson, A. D. Hamann, P. Zimmer, *Geophys. Res. Lett.* **22**, 3533 (1995).
30. G. Beutler *et al.*, *Bernese GPS Software Version 4.2* (Astronomical Institute, University of Berne, Berne, Switzerland, 2000).
31. We thank M. Schmidt and Y. Lu for their support in GPS network operations, and Central Washington University (M. Miller) and the University of Washington (A. Qamar) for providing GPS data from sites of the PANGA network, which was established with support from NSF. Supported by U.S. Geological Survey National Earthquake Hazards Reduction Program research grant 00HQGR0061; this paper is Geological Survey of Canada contribution no. 2001002. Copyright, Her Majesty the Queen in right of Canada (2001).

23 February 2001; accepted 9 April 2001
 Published online 19 April 2001;
 10.1126/science.1060152
 Include this information when citing this paper.

Age, Sex, Density, Winter Weather, and Population Crashes in Soay Sheep

T. Coulson,^{1*} E. A. Catchpole,² S. D. Albon,³ B. J. T. Morgan,⁴ J. M. Pemberton,⁵ T. H. Clutton-Brock,⁶ M. J. Crawley,⁶ B. T. Grenfell⁷

Quantifying the impact of density, extrinsic climatic fluctuations, and demography on population fluctuations is a persistent challenge in ecology. We analyzed the effect of these processes on the irregular pattern of population crashes of Soay sheep on the St. Kilda archipelago, United Kingdom. Because the age and sex structure of the population fluctuates independently of population size, and because animals of different age and sex respond in different ways to density and weather, identical weather conditions can result in different dynamics in populations of equal size. In addition, the strength of density-dependent processes is a function of the distribution of weather events. Incorporating demographic heterogeneities into population models can influence dynamics and their response to climate change.

Much recent ecological research has focused on the relative impact on population dynamics of density dependence, density-independent environmental effects, and un-

explained variation (1–3). However, to understand the mechanistic basis of population fluctuations, we also generally need to allow for the demographic structure of the

REPORTS

population (2, 4, 5). Animals of different age and sex often expend different amounts of energy at different times of the year,

associated with behavior, the costs and timing of reproductive effort, growth, and maintenance (6, 7). These differences can lead to variation in the strength and form of the association between vital rates, density, and extrinsic factors across age and sex classes. Fluctuations in the structure of the population, independent of the total population size, may then lead to interactions between density, weather, and the population structure to introduce heterogeneities that have an important impact on the population dynamics.

The size of the Soay sheep (*Ovis aries*) population on the island of Hirta in the St. Kilda archipelago off northwest Scotland fluctuates dramatically (Fig. 1A), and the dynamics can be crudely described by a nonlinear time-series (SETAR) model, which dem-

onstrates that the dynamics are a result of a nonlinear interaction between winter weather and population density (3). Although this model captures the essential features of the dynamics, the deterministic skeleton only explains 21% of the variance. To quantify interactions between density dependence, unexplained variation, and demography, we used individual-based data collected from this population between 1986 and 1996 to develop a more complex mechanistic population model. The age and sex structure of the population fluctuates more than is expected by chance and is independent of the total population size (8). Mortality rates in prime aged adults (2 to 6 years) and older adults (>6 years) are the key factors associated with the relative changes in population size (9, 10), and death is a result of starvation exacerbated by a nematode gut parasite load (11).

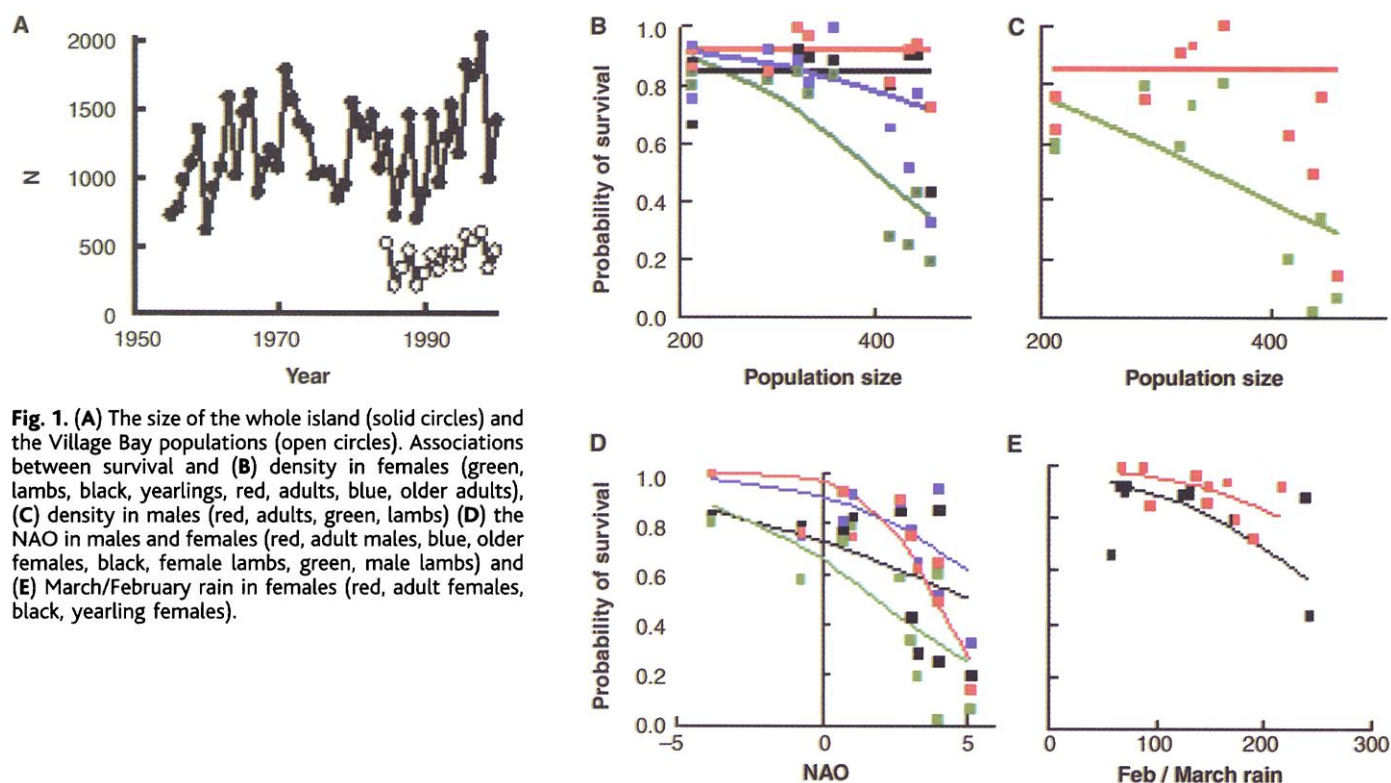
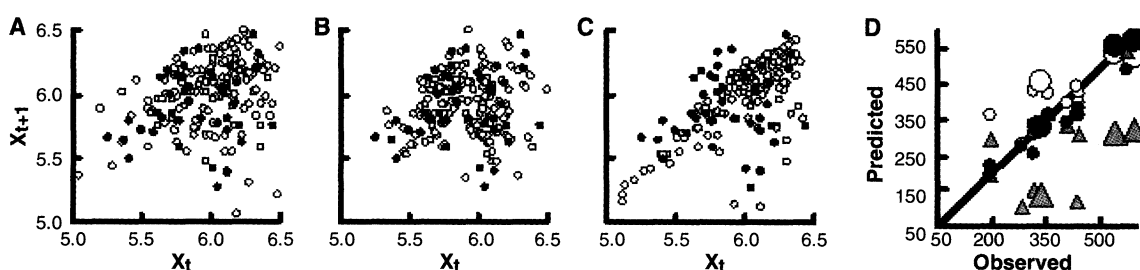


Fig. 1. (A) The size of the whole island (solid circles) and the Village Bay populations (open circles). Associations between survival and (B) density in females (green, lambs, black, yearlings, red, adults, blue, older adults), (C) density in males (red, adults, green, lambs) (D) the NAO in males and females (red, adult males, blue, older females, black, female lambs, green, male lambs) and (E) March/February rain in females (red, adult females, black, yearling females).

Fig. 2. Model of the time series. Plot of the logged population size in year $t + 1$ against the logged population size in year t for the observed time series (solid circles) and the simulated time series (open circles) for (A) the ASMM with demographic stochasticity and process noise, (B) the SETAR time-series model with process noise, and (C) the nonage-structured Markov model with demographic stochasticity and process noise. (D) The deterministic skeleton of the ASMM (solid circles) was better at capturing observed events in the time series (small symbols)



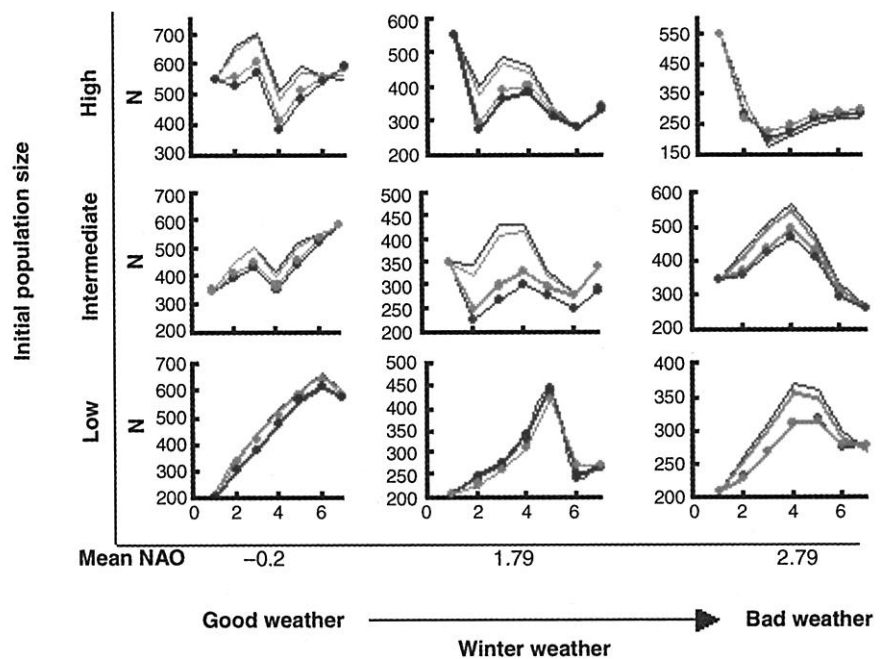
and future predictions (large symbols) than the deterministic skeletons of either the nonage-structured Markov model (open circles) or the SETAR time-series model with weather covariates (solid triangles). The line is given by $y = x$ and would designate a perfect fit (18).

REPORTS

A mark-recapture-recovery analysis (12) was conducted to explore age- and sex-specific associations between survival, density, and weather (13). Survival rates varied with age among the sexes as has been observed for other large herbivores (14), so separate analyses were conducted for males and females (12). In both sexes, survival rates of different age classes responded in contrasting ways to population density and weather (Fig. 1B) in a manner that was consistent with variation in age- and sex-specific energy expenditure (15). Survival of lambs and older females (>6 years) was negatively associated with density, whereas survival of prime adults and female yearlings was not related to density. Survival rates of lambs and males were influenced by weather throughout winter [the winter North Atlantic Oscillation (NAO) (16)], whereas survival rates of yearlings and prime adult females were most strongly influenced by rainfall at the end of winter (17). In each age and sex class, survival rates were lower in wet, windy winters (high NAO values). Density and weather interacted and bad weather depressed survival rates at high density. The strength of the interaction was greatest in young and old animals.

We combined these survival functions with those from an analysis of fecundity rates and constructed an age-structured Markov model (ASMM) (18, 19). To dissect the dynamic effects of age and sex, we compared this model with two simpler formulations: a nonage- and nonsex-structured SETAR time-series model with weather covariates (3) and a nonage-structured Markov model (19). All three models (incorporating process noise and, where appropriate, demographic stochasticity) captured the essential features of the population dynamics (Fig. 2, A through C) (20). The deterministic skeleton of the ASMM fitted the data—and captured population crashes for the time series between 1986 and 1996—better than the deterministic skeletons of either the SETAR model with weather covariates, or the nonage-structured Markov model (21) (Fig. 2D). Similarly, the ASMM was better at predicting dynamics for the period 1997 to 1999 than the SETAR model with weather covariates and the nonage-structured Markov model (22) (Fig. 2D).

The ASMM performed better than either of the simpler models because it reflects the fluctuating age and sex structure that is independent of population size, and the contrasting responses to density and different weather variables of these age and sex classes. These processes are not captured by the other models, which classify them as process noise. The influence of the demographic processes on the likelihood of population crashes occurring in the short term is shown in Fig. 3. Simulated populations of the same total initial size, experiencing



| Age/sex structure (%) | | | | | | | |
|-----------------------|--------------|------------------|---------------|---------------|------------|-------------|-------------|
| | Female lambs | Female yearlings | Female adults | Older females | Male lambs | Male adults | Older males |
| ■ | 19 | 5 | 48 | 7 | 13 | 7 | 1 |
| ▨ | 17 | 8 | 41 | 8 | 18 | 8 | 0 |
| ● | 23 | 10 | 24 | 11 | 19 | 13 | 0 |
| ● | 22 | 13 | 17 | 13 | 16 | 19 | 0 |

Fig. 3. The age and sex structure of the population influences the dynamics. Each individual graph displays the result of four simulations with identical weather conditions and initial starting population size. In each graph, each line represents one simulation with different initial age and sex structure chosen from the data (below). The y axis shows different starting population sizes, and the x axis different mean values for the simulated weather distributions.

identical weather regimes but with different initial age and sex structures, have different trajectories. The greater the proportion of animals in the population whose probability of survival is associated with density (lambs and older females) and those whose survival is most strongly associated with weather (lambs, males, and older females) (Fig. 1B), the more likely the population is to decline from high or intermediate densities. The effect of population structure on the dynamics is strongest at high and intermediate initial population sizes and weakest when the population is low (Fig. 3). This is because there is more variation across age and sex classes in survival rates, which drive population crashes, than there is in fecundity rates, which underpin population increases. These results underline the importance of incorporating the age and sex structure of the population into models.

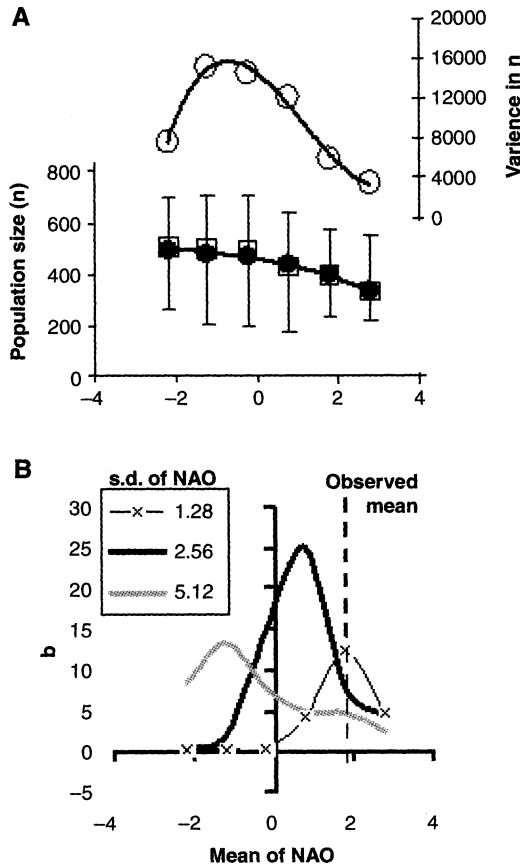
The population's demographic structure de-

pends on the population and environmental history as well as on the current population size and weather. Thus the age and sex structure can differ markedly in years with identical population size and weather. Any attempt to predict future population size or the effects of climate change in this or similar systems must therefore take account of the age and sex structure.

We also explored how weather and density interact to influence the longer term pattern of population fluctuations. Specifically, we examined how the dynamics varied with the distributions of the weather. As the mean value of the NAO and February and March rain increases, and as the winter weather becomes wetter and stormier, the mean and median population size declines (Fig. 4A). In contrast, the variance in population size follows a humped distribution with lower variation in population size when the weather is either very wet and stormy, or very dry (Fig. 4A).

REPORTS

Fig. 4. The pattern of population fluctuations varies as a function of the distribution of weather events. **(A)** The mean and median of simulated population sizes decreases as winter weather gets progressively wetter and stormier. The range of observed averages calculated over 10-year periods. The bars represent maximum and minimum values. The variance in population size follows a humped distribution with most variation in population size occurring when the weather is slightly drier than the observed mean. **(B)** We varied the mean \pm SD for the simulated weather distributions (observed NAO variance = 2.56) and fitted the curve $N_{t+1} = aN_t / (1 + cN_t^b)$ to the simulation results. As the value of the parameter b increases, the degree of density-dependent overcompensation increases. The distribution of b varies with the mean \pm SD of the weather distribution. When the weather is good (NAO < -1) or bad (NAO > 2), the dynamics do not exhibit overcompensatory density dependence. For the observed level of fecundity, values of $b > 21$ would produce chaotic dynamics in the associated simple deterministic model (24).



Finally, we explored how the degree of density-dependent overcompensation underlying this pattern (23, 24), and consequently the frequency and magnitude of population declines, varied with the mean severity and variability in the weather distributions (25) (Fig. 4B). The degree of overcompensation followed a humped distribution with increasing NAO. Overcompensatory density dependence was greatest for intermediate mean values of the NAO. When the weather is, on average, good (low NAO values), the weather is rarely severe enough to cause crashes. When the weather is, on average, very bad, the population never reaches a large enough size for dramatic density-dependent declines to occur. Between these two climatic extremes, apparent overcompensation reaches its maximum (the deterministic skeleton may even be driven into the chaotic region), and the dynamics enter a regime when sheep population crashes occur. In this regime, generally good climatic conditions allow the population (and its mean age) to increase, then a bad winter interacts with density and demography to produce a crash.

Because one of the features of the NAO is a decadal trend of cold, dry winters followed by wetter, stormier winters (16), our results suggest that the population dynamics of the Soay sheep are likely to alternate between periods when the dynamics are overcompensatory and

periods when they are not. This suggests that global climate change is likely to alter the dynamic properties of the system.

As more data on individual life histories have become available for the Soay sheep population, our understanding of the dynamics has evolved from a view of strict cyclic dynamics as a result of overcompensatory nonlinear density-dependent determinism (22) through an interaction between nonlinear density dependence and environmental stochasticity (3) to the current picture: a nonlinear interaction between density, weather, and population structure. By demonstrating this interaction, we have shown why environmental variation is important biologically and that simple time-series models do not allow accurate predictions of age- and sex-structured populations. The ability to accurately predict future population sizes is crucial for a range of epidemiological, conservation, and management problems, and because Soay sheep closely fit the demographic pattern reported for many large herbivores (14), the processes we describe are likely to exist across a wide range of large herbivore populations.

References and Notes

1. O. N. Bjørnstad, J. M. Fromentin, N. C. Stenseth, J. Gjøsaeter, *Proc. Natl. Acad. Sci. U.S.A.* **96**, 5066 (1999).
2. H. Leirs et al., *Nature* **389**, 176 (1997).
3. B. T. Grenfell et al., *Nature* **394**, 674 (1998).

4. R. Hilborn, M. Mangel, *The Ecological Detective: Confronting Models with Data* (Princeton Univ. Press, Princeton, NJ, 1997).
5. G. Caughley, *Analysis of Vertebrate Populations* (Wiley, London, 1977).
6. S. C. Stearns, *The Evolution of Life History Strategies* (Oxford Univ. Press, Oxford, 1992).
7. T. H. Clutton-Brock, Ed. *Reproductive Success: Studies of Individual Variation in Contrasting Breeding Systems* (Univ. of Chicago Press, Chicago, IL, 1988).
8. Results obtained by simulation (26).
9. T. Coulson, S. Albon, J. Pilkington, T. Clutton-Brock, *J. Anim. Ecol.* **68**, 658 (1999).
10. P. Grubb, in *Island Survivors: the Ecology of Soay Sheep on St. Kilda*, P. A. Jewell, C. Milner, J. M. Boyd, Eds. (Athlone, London, 1974), pp. 242–272.
11. F. M. D. Gulland, *Parasitology* **105**, 493 (1992).
12. E. A. Catchpole, B. J. T. Morgan, T. N. Coulson, S. N. Freeman, S. D. Albon, *Appl. Stat.* **49**, 453 (2000).
13. J. M. Milner, D. A. Elston, S. D. Albon, *J. Anim. Ecol.* **68**, 1235 (1999).
14. J. M. Gaillard, M. Festa-Bianchet, N. G. Yoccoz, A. Loison, C. Toigo, *Annu. Rev. Ecol. Syst.* **31**, 367 (2000).
15. Males and females expend different amounts of energy in reproduction in autumn and spring, and young animals expend more energy on growth than adults (26).
16. J. W. Hurrell, *Science* **269**, 676 (1995).
17. Wetting of an animal's coat is energetically expensive because it reduces resistance to heat flux by a factor of 2. Rainfall values from 1986 to 1996 were obtained from the meteorological station at Benbecula, Scotland. The station was closed in July 1996 so local weather values since then were estimated by extrapolating from the 1986 to 1996 correlation between the monthly weather averages for Benbecula and Stornway, Scotland. There was no significant temporal autocorrelation in the weather between 1986 and 1996.
18. S. Tuljapurkar, H. Caswell, *Structured-Population Models in Marine, Terrestrial, and Freshwater Systems* (Chapman & Hall, New York, 1997).
19. The ASMM is a stochastic matrix model incorporating age- and sex-specific survival and fecundity functions. The nonage-structured Markov model incorporates survival functions for males and females independent of age, and a female fecundity function (26).
20. The performance of the stochastic formulations of the three models was assessed by comparing the means, variances, and sums of squares of the simulated series with observations (26).
21. The r^2 values of prediction versus observation were 0.92, 0.67, and 0.54 for the deterministic skeletons of the age-structured Markov model, the SETAR time-series model with weather covariates, and the nonage-structured Markov model, respectively, mean absolute error $e = \sum[\text{abs}(\text{obs} - \text{exp})]/n = 46.2, 103.0,$ and 46.9 respectively.
22. Statistics for the predictions of the age-structured Markov model, the SETAR time-series model, and the nonage-structured Markov model: $r^2 = 0.99, 0.38,$ and 0.85 and $e = 11.3, 63.9,$ and 231 .
23. B. T. Grenfell, O. F. Price, S. D. Albon, T. H. Clutton-Brock, *Nature* **355**, 823 (1992).
24. M. P. Hassell, J. H. Lawton, R. M. May, *J. Anim. Ecol.* **45**, 471 (1976).
25. We defined the degree of density-dependent overcompensation as the size of the parameter b for the population model $N_{t+1} = \lambda d N_t / (1 + (a N_t)^b)$ fitted to a simulated time series, where $a, b,$ and d are average survival parameters, and $\lambda = (f + 1)$, where f is the average individual reproductive rate (23, 24). Simulated time series were scaled by dividing by the mean of N_t .
26. Supplementary material is available on Science online at www.sciencemag.org/cgi/content/full/292/5521/1528/DC1.
27. We thank the National Trust for Scotland and the Scottish Natural Heritage for permission to work on St. Kilda, and the Royal artillery for logistical support. We also thank J. Pilkington, A. McColl, A. Robertson, and the many volunteers for collecting data, and O. Bjørnstad, S. Freeman, M. Forschammer, A. Illius, J. Linstrom, I. Stevenson, and K. Wilson for comments.

31 January 2001; accepted 4 April 2001